# Evolution of microstructure in spray formed Al–18%Si alloy

V.C. Srivastava [a,*], R.K. Mandal [b], S.N. Ojha [b]

[a] *Materials Processing Division, National Metallurgical Laboratory, Jamshedpur 831007, India*
[b] *Department of Metallurgical Engineering, Banaras Hindu University, Varanasi 221005, India*

## Abstract

Spray atomization and deposition process has emerged as an alternative to ingot and powder metallurgy routes. In the present investigation, we study the microstructural control during spray deposition of hypereutectic Al–Si alloy, employing different nozzle to substrate distances. Spray deposition is carried out using convergent–divergent close-coupled nozzle design at deposition distances of 200, 300, 450, and 550 mm. Microstructural characterization of oversprayed powders as well as spray formed deposits was performed. Microstructural features obtained at smaller deposition distance consist of co-existing primary Si phase and needle like eutectic Si. Dendrites of α-Al phase are observed indicating a large undercooling of the liquid pool prior to solidification. A large number of pre-solidified particles with very fine microstructure, embedded in a relatively coarse region, typically characterize those evolved at large deposition distances. However, at intermediate deposition distances, uniform and refined primary Si phases, 3–8 μm size, are observed. An undercooling effect is manifested in both the spray deposits as well as powder particles. These microstructural features have been discussed in light of a proposed model, which describes the presence of two layers (1) solidification layer and (2) interaction layer in the liquid pool.
© 2004 Elsevier B.V. All rights reserved.

*Keywords:* Spray deposition; Microstructure; Phase; Hypereutectic Al–Si; Undercooling

## 1. Introduction

Aluminium–Silicon alloys possess high strength to weight ratio, low thermal expansion coefficient, and high wear resistance. These alloys also show improved strength and wear properties as the silicon content is increased above eutectic composition. Such properties warrant the use of these materials as structural components in automotive industries. However, the large polyhedral shape of primary Si and coarse needle shape of eutectic silicon (Si) present in the conventionally cast hypereutectic alloys deteriorate their mechanical properties. In general, the refinement of primary phase and modification of eutectic are achieved by addition of small amounts of grain refiners such as phosphorous, and modifiers like sodium, strontium and other rare earth elements during casting [1,2]. Alternatively, rapid solidification processing (RSP), following melt atomization, has shown considerable refinement and modification

of the constituent phases with inherent homogeneity of the microstructure [3–5]. However, powder particles require consolidation by hot extrusion or hot isostatic pressing. Consequently, the number of processing steps are increased.

Some of the problems of RSP route of materials processing are overcome in spray deposition processing. The process involves atomization of a liquid metal into a spray of micron-sized droplets using a high velocity inert gas jet. The spray is subsequently deposited on a stationary or moving substrate to produce a near net shape preform. Refinement in microstructure with equiaxed morphology of primary phase and considerable chemical homogeneity are typical features of spray formed alloys [4–6].

There are several investigations on the spray forming of Al–Si alloys [7–12], however, a detailed study on the effect of deposition distance on their microstructural features are not clearly evaluated. The present investigation studies the microstructural characteristics of Al–18 wt.%Si alloy, spray deposited at different nozzle to substrate distances. These characteristics have been discussed in light of thermal conditions of spray before deposition, during deposition, and various mechanisms prevalent during solidification of the deposit.

---

* Corresponding author. Tel.: +91-657-2271709ext. 2201;
fax: +91-657-2270527.
*E-mail addresses:* vcsrivas@nmlindia.org, vcsrivas@yahoo.com
(V.C. Srivastava).

## 2. Experimental details

The details of spray forming process used in the present investigation have been described elsewhere [13]. In brief, the process makes use of an annular convergent–divergent nozzle concentric to a melt delivery tube to generate a spray of micron-sized droplets. The gas–melt interaction in this process occurs at the tip of the flow tube. The spray deposition is carried out in an environmental chamber. The alloy with composition Al–18 wt.%Si was melted in a graphite crucible using a resistance heating furnace. The melt temperature was controlled within an accuracy of $\pm 2\,^{\circ}$C. A melt superheat of 200 $^{\circ}$C was invariably maintained in the crucible in all the experiments to prevent premature freezing of the melt during spray atomization. The melt was subsequently poured in a tundish fitted with the spray nozzle at its bottom. The flow of gas was initiated to atomize the melt. The spray of droplets was deposited over a steel substrate. In the present work, four sets of experiments were conducted with nozzle to substrate distances $(Z_{N \rightarrow S})$ of 200 mm (deposit-A), 300 mm (deposit-B), 450 mm (deposit-C) and 550 mm (deposit-D). The gas pressure of 1.2 MPa with gas flow rate of 1.75 kg min$^{-1}$ and melt mass flow rate of 1.78 kg min$^{-1}$ were consistently maintained during atomization.

The samples of oversprayed powder particles as well as spray deposits were prepared for microstructural investigation using standard metallographic techniques and were etched with Keller's reagent (1 vol.% hydrofloric acid, 1.5 vol.% hydrochloric acid, 2.5 vol.% nitric acid and rest water) at room temperature for 30 s. The microstructures were examined under Leitz optical microscope. The size and size distribution of primary Si phase were measured using a VIDS image analyzer. An area of 0.032 mm$^2$ was taken for each measurement and a total of 100 measurements were taken for each data point.

## 3. Results

The microstructure of oversprayed powder particles of Al–18 wt.%Si alloy shows two distinct morphologies. The large sized particles clearly show fine primary Si phase evenly distributed in the matrix phase (Fig. 1a). Whereas, smaller particles depict development of $\alpha$-Al phase at the surface of primary Si particulates (Fig. 1b). The microstructure away from the dendrites has eutectic morphology with needle shape Si.

The microstructure of deposit-A shows regions of distinct morphological features. One of the regions show fine and uniformly distributed primary Si particulates co-existing with small needle shaped eutectic Si phase (Fig. 2a). Whereas, the other region reveals distinct $\alpha$-Al dendrites together with eutectic phase (Fig. 2b). Particulates of primary Si phase are not observed in the latter. This microstructural feature is not expected from Al–18%Si alloy solidified under equilibrium condition. The microstructure near the substrate/preform interface does not exhibit these features, except very fine primary Si phase.

As the deposition distance is increased to 300 mm (deposit-B), the size of the primary Si phase is reduced and eutectic Si is modified to its globular shape (Fig. 3a). Some of the regions indicate clustering of Si particulates in this deposit. It has also been observed that the bottom layer of the preform consists of a very fine microstructure with around 2.5 μm size Si particulates and is clearly demarked from the rest of the preform (Fig. 3b). The size of this layer is around 150 μm. This is a transient layer due to a high cooling rate in the initial stages of deposition.

Further increase in the deposition distance (deposit-C) led to reduction in primary Si size and gave rise to a more uniform spatial distribution of particulates. However, a few characteristic flow bands are seen in this deposit. A typical microstructure showing flow bands is shown in Fig. 4. The interesting feature of this band is the scale of microstructure on the two sides of the band. On the one side it is very fine, while on the other it acquires coarser microstructure. The flow band is highly dense in primary Si phase. The microstructural variation through preform thickness shows that the size of primary Si particulates initially increases rapidly with distance from preform bottom and then attains a steady state i.e. constant size, and further there is a decrease in size precisely in the top layer of the preform (Fig. 5). These measurements are related to the
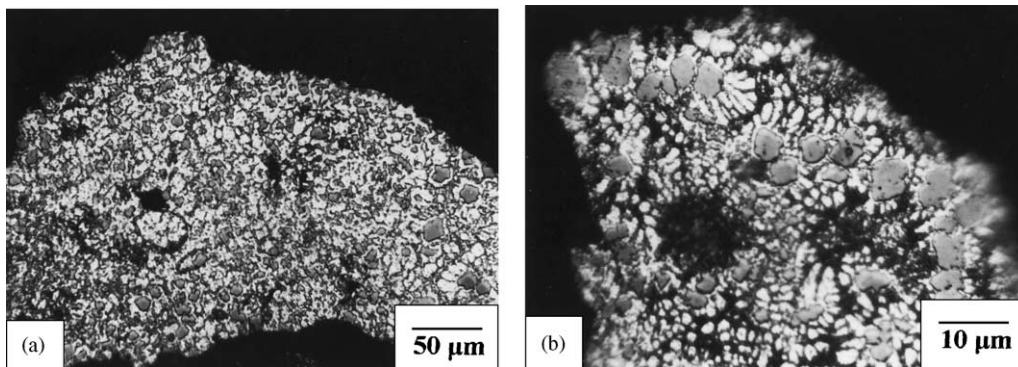


Fig. 1. Micrographs of oversprayed powder particles showing (a) large size particle with primary Si phase (b) extensively undercooled smaller particle with $\alpha$-Al dendrites.
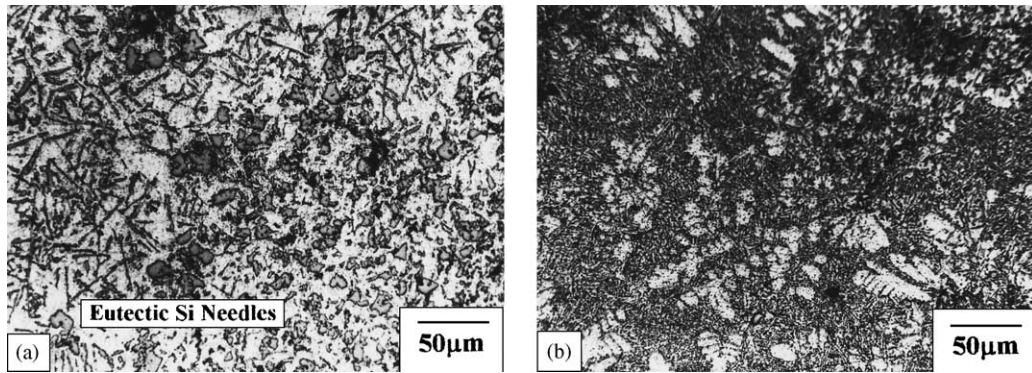
Fig. 2. Micrographs of spray deposit produced at $Z_{N \to S} = 200$ mm showing (a) fine primary Si co-existing with fine eutectic Si needles (b) dendrites of $\alpha$-Al phase.
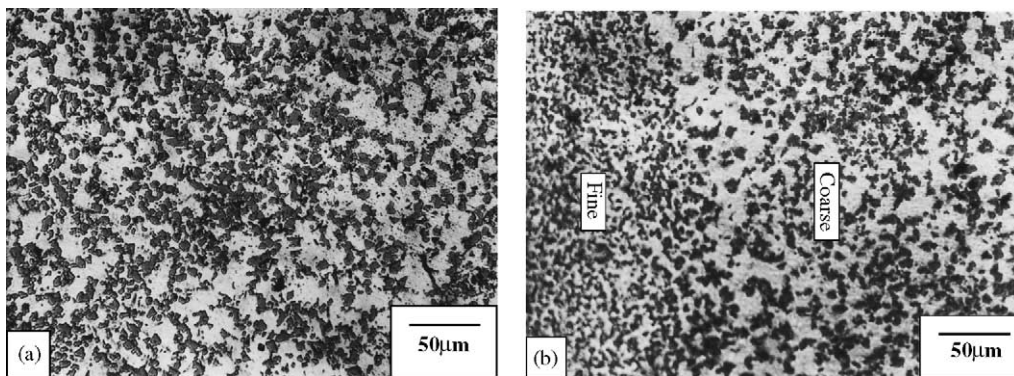


Fig. 3. Micrographs of spray deposit produced at $Z_{N \to S} = 300$ mm showing (a) globular shape of fine primary Si phase (b) transient layer at the bottom of the preform.

spray deposit-B and -C. The size distribution of primary Si in different regions of the preform was akin to a Gaussian shape. It is clear that the size of Si particulates in deposit-B is larger compared to that in deposit-C as evident in Fig. 5. The size remains constant in the steady state condition.

The microstructural feature of deposit-D shows fine undeformed powder particles of around 20 μm size embedded even in the central regions of the preform (Fig. 6). Prior particle boundaries were noticeable with very fine Si partic-

ulates within the pre-solidified particles. The boundaries of the particles are not clearly delineated but the scale of microstructure within these particles maintains their identity in relatively coarser surrounding areas. These features have been found to increase considerably towards the peripheral regions of the deposit. Peripheral regions invariably showed large number of pre-solidified particles attached to each other leaving interstices.
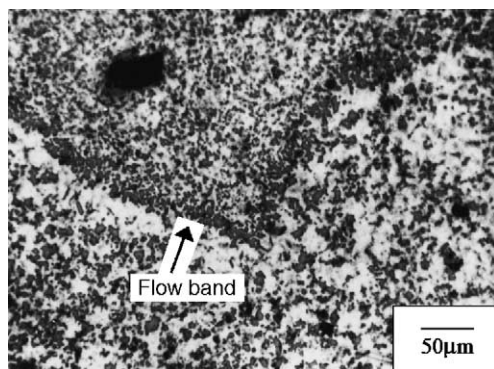


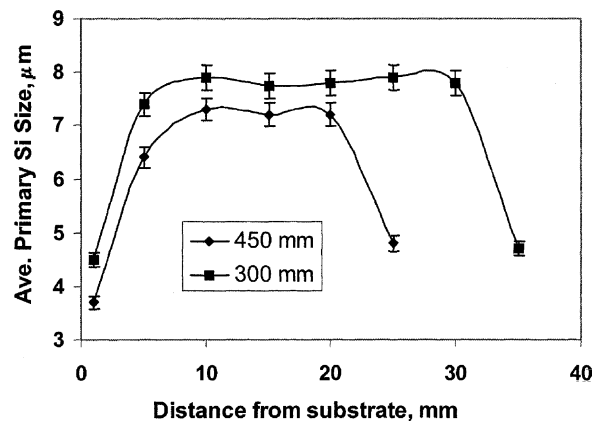Fig. 4. Flow bands observed in spray deposit produced at $Z_{N \to S} = 450$ mm.



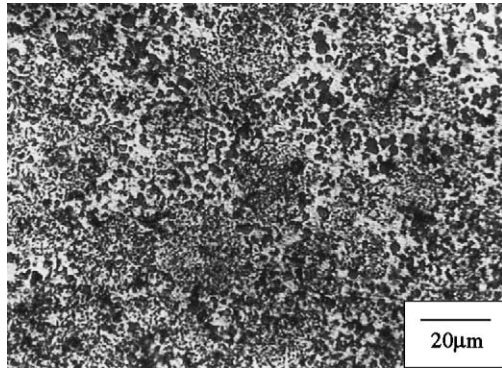Fig. 5. Variation of primary Si size along the thickness of the deposit produced at $Z_{N \to S} = 300$ and 450 mm.

Fig. 6. Pre-solidified particles in a relatively coarser matrix observed in the central region of the spray deposit produced at $Z_{N \to S} = 550$ mm.

## 4. Discussion

### 4.1. Droplet undercooling

The above microstructural characteristics can be qualitatively understood in light of the thermal conditions of droplets before impingement on the substrate surface and their interaction with the growing surface of the preform. A wide size range of micron-sized droplets is created during atomization that is subsequently deposited on the substrate. These droplets experience a high cooling rate of the order of $10^3$–$10^5$ $^\circ$C s$^{-1}$ by a convective mode of heat transfer through the high velocity carrier gas jet during flight [14]. The cooling rate of droplets depends upon specific droplet/gas interface area. It is obvious from the micrograph (Fig. 1b) of the powder particle that smaller particles experience extensive undercooling. This statement is validated keeping in view that such a microstructure can only be evolved when the solidifying liquid is undercooled. Extensive nucleation and growth of primary Si, at the commencement of solidification in undercooled state, leaves its vicinity devoid of Si and the composition around Si particulate reaches to hypoeutectic region of equilibrium phase diagram [11]. Owing to high cooling rate and undercooled state of smaller droplets a large compositional gradient is formed away from the interface. As a result, the primary $\alpha$-Al phase nucleates at the interface. The growth of $\alpha$-Al dendrites is accompanied with rejection of solute and the composition away from the dendrite interface reaches to coupled eutectic regime. Therefore, further solidification takes place in that region. These features are distinct in the given micrograph. Therefore, it can be concluded that a smaller droplet undergoes large undercooling compared to bigger ones. Different size droplets experience different degrees of undercooling. A large flight time for droplets ensures that solidification starts prior to impingement on the substrate. Whereas, a small flight time will lead the droplets to reach the substrate in undercooled state.

### 4.2. Microstructure development in the deposit

At the beginning of deposition process, the droplets splat on the substrate and experience a high cooling rate that depends upon the thermal conductivity of the substrate and its temperature. Therefore, the deposit exhibit a fine microstructure in the vicinity of the substrate (Fig. 3b). The heat transfer by convection at this stage remains insignificant as most of the heat transfer takes place by conduction through the substrate. As the thickness of the deposit increases, the temperature gradient within the growing preform becomes smaller as well as the substrate temperature rises. As a result, heat transfer by conduction becomes slow and a large fraction of heat removal is achieved by convective mode of heat transfer, and a liquid pool builds up in the top layer of the growing preform. The thickness of this pool increases with increase in the deposit thickness until a steady state condition is achieved. This corresponds to a situation when heat transfer through the substrate becomes insignificant compared to heat removal by forced convection. The transient thickness of deposit before the onset of steady state depends mainly on the conductivity of the substrate, conductivity of the deposited material and arrangements employed for the cooling of the substrate. Solidification of liquid pool under steady state condition gives rise to uniform microstructural features in the preform. However, the fine microstructure in the vicinity of the substrate experiences a longer high temperature exposure due to heat flow during further deposition period. As a result, the microstructure becomes slightly coarser but not comparable to that observed in the steady state condition. High momentum transfer from the droplets creates a turbulent fluid flow condition apart from the fragmentation of solid phases existing in the droplets as well as in the solidifying liquid pool. The two processes concurrently lead to refinement and modification of microstructure in the preform [9,10,15,16]. In addition, constrained growth at reduced temperature, inherent in spray deposition process, leads to finer microstructure [17].

A large flight time for the droplets in the spray renders lower enthalpy content to the spray prior to deposition. However, as mentioned above, if the deposition distance is smaller, a large fraction of the large size droplets comes on the growing preform in undercooled state. Since the central region of the spray consists of larger size droplets [4,5,18], this region receives highly undercooled droplets. This has also been suggested by Xu and Lavernia [19] and Ojha et al. [9]. The model from Shukla et al. [20] shows that a 120 $\mu$m droplet remains in undercooled state up to 300 mm deposition distance. The formation of $\alpha$-Al dendrite co-existing with eutectic and also the formation of small eutectic Si needles with refined primary Si phase corroborate the qualitative observation that the liquid pool also remains in undercooled state at smaller $Z_{N \to S}$. The above two microstructural features (Fig. 2a and b) can only be possible if there are regions with different degrees of undercooling. This has been demonstrated by Srivastava et al. [11] by heat treating the
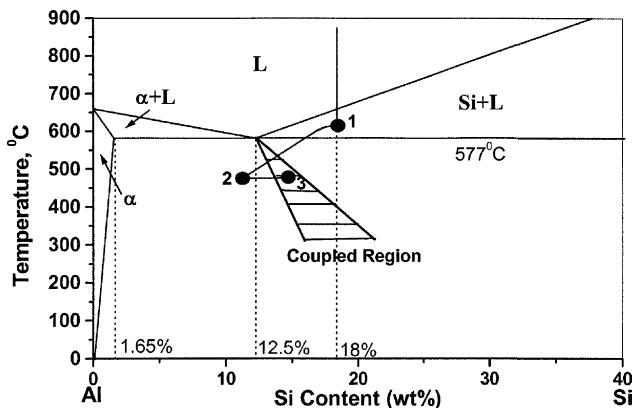
Fig. 7. An schematic of equilibrium phase diagram showing path of compositional change during solidification of undercooled melt.

deposits in semi-solid region of equilibrium phase diagram. A typical solidification route for an undercooled liquid is shown in Fig. 7. The commencement of nucleation of primary Si takes place at position 1. As a result, the solute content decreases ahead of the interface, between primary phase and remaining liquid, leading the composition to reach in the hypoeutectic region (position 2). Further solidification of liquid gives rise to the nucleation of primary $\alpha$-Al phase and simultaneous rejection of Si. Therefore, the solute content in the liquid reaches to asymmetric coupled region (position 3) giving rise to eutectic microstructure. However, a turbulent fluid flow condition in the interaction domain, during deposition, does not allow formation of dendrites or needles. This is the basis of equiaxed grain morphology in the spray deposition process [4]. Therefore, the above discussion cannot justify the current microstructural observation. Hence, a new solidification model is proposed in this study.

### 4.3. Solidification model

The microstructural features can be understood by considering the liquid pool thickness at different deposition distances ($Z_{N\rightarrow S}$). The liquid pool thickness increases with decrease in deposition distance, when all other parameters are kept constant [4]. The liquid pool thickness also varies during deposition process. At the beginning and at the end of the process, when cooling rate is high, liquid pool thickness is small. Whereas, the thickness in steady state condition is basically governed by the deposition distance. The microstructural analysis given in this paper, and corroborated with the present solidification model, is done for those microstructures obtained from the middle sections of the deposit. This section is expected to represent the steady state. Fig. 8 shows a model for solidification of the preform. This depicts the existence of a liquid pool or solidification layer, the thickness of which has been termed as $L_s$. The interaction layer ($L_i$) has been defined, in conformity with Liang and Lavernia [21], as the depth of liquid pool up to which the effect of momentum transfer from the droplets is experienced. The layer below the interaction layer remains undisturbed by momentum transfer. At a smaller value of $Z_{N\rightarrow S}$, the formation of flake like eutectic Si and relatively coarser primary Si in deposit-A can be understood by the fact that a large liquid fraction and, thus, thicker liquid pool is obtained at a smaller deposition distance of 200 mm. Further, such a thick liquid pool restricts the interaction layer ($L_i$) to a height less than the solidification layer ($L_s$). Owing to cushioning effect of the former, which does not allow the momentum transfer from droplets to the lower part of the solidification layer, the undisturbed layer ($L_s - L_i$) experiences a solidification condition akin to that of the normal casting that leads to the growth of eutectic Si as needles (Fig. 2a). This features is not observed at the bottom and the top of the deposit as the liquid pool thickness is small
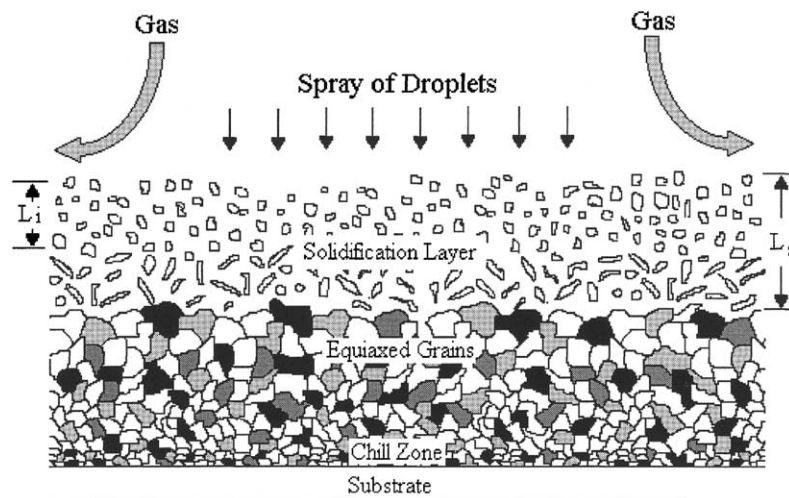


Fig. 8. The proposed model of the deposit solidification depicting an interaction layer and a solidification layer.

and there exist no cushioning effect by liquid pool. Liquid splashing at the top layer by high velocity gas may add to reduction of $L_s$ depending upon $Z_{N \to S}$. It has been reported by Srivastava and Ojha [22] that the axial gas velocity up to 200 mm distance from the nozzle exit remains $100 \, \text{ms}^{-1}$.

Further decrease in the incoming enthalpy, at larger deposition distance, gives rise to smaller $L_s$ and larger solid fraction in the spray and a large fraction of droplets reach the substrate in semi-solid state. The limited volume fraction of liquid available on the deposition surface leads to a condition of constrained growth and, thus, smaller size of primary Si particulates is obtained. Flakelike eutectic Si and primary $\alpha$-Al dendrites observed in the deposit-A do not form in deposit-B because the top surface of growing preform does not receive undercooled droplets as the flight distance increases. Furthermore, solidification layer becomes comparable to the interaction layer with decrease in the liquid fraction in the spray with increasing deposition distance. A decrease in the Si size in deposit-C has been attributed to subsequent decrease in the liquid fraction and, thus, lower solidification time. Further increase in deposition distance $Z_{N \to S}$ (deposit-D) leads to a drastic decrease in the liquid fraction and the individual pre-solidified particles ($\approx 50 \, \mu m$) with very fine microstructure are observed in relatively coarser matrix (Fig. 6). A low liquid fraction permits only surface re-melting of these particles. Therefore, the identity of the particles is confirmed only by their finer microstructure. The possibility of finding pre-solidified particles exists at each deposition distance but the critical size of the particles increases as the deposition distance is increased. It has been observed that for larger $Z_{N \to S}$, the pre-solidified particle volume fraction is prevalent both in the centre and the periphery of the deposit. However, as $Z_{N \to S}$ decreases, pre-solidified particles are mostly located at the periphery and for $Z_{N \to S} = 200 \, \text{mm}$, pre-solidified particles are not discernible. Large liquid fraction and high heat content at smaller values of $Z_{N \to S}$ may result in re-melting of particles and thus pre-solidified particles are seldom observed for deposit-A. At moderate to low liquid fraction for deposit-C, the surface of the particles may act as nucleation site for crystallization of remaining liquid phase [10,19]. At the end of each deposition process, when the heat input is stopped, a high cooling rate is experienced in the top layer of the preform compared to its interior. The reduction in the primary Si size at the top of the preform, after steady state Si size in deposit-B and deposit-C, has been attributed to this phenomenon.

Flow bands with high density of primary Si phase particulates and with two scales of microstructures on either side of the band are observed only in deposit-C (Fig. 5). There are quiet a few number of these bands in regions slightly away from the centre of the preform. The presence of any pre-solidified particle, around which nucleation would have started, is ruled out considering the size of the band. Therefore, these features could only be attributed to turbulent fluid flow conditions prevailing during solidification of the pre-

form. Such a flow band would be visible only when there is locally inhomogeneous liquid content in different regions of the preform. Such a condition is met in the present case for deposit-C. As discussed earlier, at $Z_{N \to S} = 450 \, \text{mm}$, preform receives moderate to low liquid fraction that does not allow uniformity of liquid phase in the top layer of the growing preform. In this process, relative movement of liquid phase could be delineated in the form of flow lines. In addition, the high density of primary Si phase in the flow band results from one or both of the two reasons: (1) formation of a boundary layer in the vicinity of relatively solid phase, which leads to accumulation of already grown Si particulates at the boundary and (2) nucleation of primary Si phase on the solid surface, which is less probable at low liquid fractions. This argument can be validated by the presence of pre-solidified particles at 550 mm of deposition distance.

## 5. Conclusions

The microstructure of the spray deposited Al–18 wt.% Si alloy is drastically affected by nozzle to substrate distance. At smaller deposition distance of 200 mm, $\alpha$-Al dendrites and needle like constituent of eutectic Si phase are observed. This has been attributed to large undercooling experienced by the liquid pool. At large nozzle to substrate distance of 550 mm, well defined pre-solidified particles are observed. A uniform and refined microstructure is evolved at intermediate distances. These variations have been attributed to the difference between interaction layer and the solidification layer in the top of the growing preform. A controlled microstructure can be obtained when $L_s$ and $L_i$ are comparable.

## References

[1] N. Tenekedjiev, J.E. Gruzleski, Cast Met. 3 (2) (1990) 96.
[2] M. Adachi, J. Jpn. Inst. Light Met. 4 (7) (1984) 430.
[3] E.J. Lavernia, Int. J. Rapid Solidification 5 (1) (1989) 47.
[4] E.J. Lavernia, Y. Wu, Spray Atomization and Deposition, Wiley, West Sussex, England, 1996, p. 487.
[5] E.J. Lavernia, J.D. Ayers, T.S. Srivatsan, Int. Mater. Rev. 37 (1) (1992) 1.
[6] P.S. Grant, Prog. Mater. Sci. 39 (1995) 497.
[7] W. Kahl, J. Leupp, Met. Powder Rep. 45 (4) (1990) 274.
[8] J.L. Estrada, J. Duszczyk, J. Mater. Sci. 25 (1990) 1381.
[9] S.N. Ojha, J.N. Jha, S.N. Singh, Scripta Met. Mater. 25 (1991) 443.
[10] V.C. Srivastava, R.K. Mandal, C. Ramachandra, B. Chatterjee, S.N. Ojha, Trans. Ind. Inst. Met. 51 (1) (1999) 49.
[11] V.C. Srivastava, R.K. Mandal, S.N. Ojha, J. Mater. Sci. Lett. 20 (1) (2001) 27.
[12] V.C. Srivastava, P. Ghosal, S.N. Ojha, Mater. Lett. 56 (2002) 797.
[13] S.N. Ojha, A.K. Tripathi, S.N. Singh, Powder Met. Int. 25 (1993) 65.
[14] A.K. Srivastava, S.N. Ojha, S. Ranganathan, Met. Mater. Trans. A 29 (8) (1998) 2205.
[15] V.C. Srivastava, A. Upadhyay, S.N. Ojha, Bull. Mater. Sci. 23 (2) (2000) 73.
[16] Y. Wu, W.A. Cassada, E.J. Lavernia, Met. Mater. Trans. A 26 (5) (1995) 1235.

[17] S. Annavarapu, R.D. Doherty, Acta Metall. Mater. 43 (8) (1995) 3207.

[18] V.C. Srivastava, R.K. Mandal, S.N. Ojha, in: Proceedings of the International Conference on Spray Deposition and Melt Atomization (SDMA-2000), Bremen, Germany, 25–28 June 2000, Druckerei der Universität Bremen, Bremen, 2000, p. 855.

[19] Q. Xu, E.J. Lavernia, Scripta Metall. Mater. 41 (1999) 535.

[20] P. Shukla, V.C. Srivastava, R.K. Mandal, S.N. Ojha, in: Proceedings of the International Conference on Solidification Science and Processing: Outlook for 21st Century, Banaglore, India, 18–21 February 2001, Trans. Tech. Publisher, Switzerland, 2001, p. 1.

[21] X. Liang, E.J. Lavernia, Metall. Mater. Trans. A 25 (11) (1994) 2341.

[22] V.C. Srivastava, S.N. Ojha, P/M Sci. Technol. Briefs 3 (3) (2001) 5.